Dan Zhu,[1] Li Xie,[1] Youhou Kang,[1] Subhankar Dolai,[1] Jakob Bondo Hansen,[1] Tairan Qin,[1] Huanli Xie,[1] Tao Liang,[1] Deborah C. Rubin,[2,3] Lucy Osborne,[1,4] and Herbert Y. Gaisano[1]

Syntaxin 2 Acts as Inhibitory SNARE for Insulin Granule Exocytosis

Diabetes 2017;66:948–959 | DOI: 10.2337/db16-0636

Of the four syntaxins specialized for exocytosis, syntaxin (Syn)-2 is the least understood. In this study, we used Syn-2/epimorphin knockout mice to examine the role of Syn-2 in insulin secretory granule (SG) exocytosis. Unexpectedly, Syn-2 knockout mice exhibited paradoxical superior glucose homeostasis resulting from an enhanced insulin secretion. This was confirmed in vitro by pancreatic islet perifusion showing an amplified biphasic glucose-stimulated insulin secretion arising from an increase in size of the readily releasable pool of insulin SGs and enhanced SG pool refilling. The increase in insulin exocytosis was attributed mainly to an enhanced recruitment of the larger pool of newcomer SGs that undergoes no residence time on plasma membrane before fusion and, to a lesser extent, also the predocked SGs. Consistently, Syn-2 depletion resulted in a stimulation-induced increase in abundance of exocytotic complexes we previously demonstrated as mediating the fusion of newcomer SGs (Syn-3/VAMP8/SNAP25/Munc18b) and predocked SGs (Syn-1A/VAMP2/SNAP25/Muncn18a). This work is the first to show in mammals that Syn-2 could function as an inhibitory SNARE protein that, when relieved, could promote exocytosis in pancreatic islet β-cells. Thus, Syn-2 may serve as a potential target to treat diabetes.

ISLET STUDIES

Exocytosis of insulin secretory granules (SGs) from pancreatic β-cells (1) mimics neurotransmitter release (2), with major components of the neuronal exocytotic fusion machinery, including the three SNARE proteins—syntaxin (Syn)-1A, SNAP-25, and VAMP-2—and nSec/Munc18 (SM) protein Munc18a, which acts to remodel and activate SNARE complex assembly. β-Cells, unlike neurons, use several modes of exocytosis from several SG pools to mediate a biphasic insulin secretory pattern that drives glucose uptake during a meal (3). Vesicle SNARE (v-SNARE; VAMP-2 and -8) and target membrane SNARE (Syn-1A through Syn-4 and SNAP25) and SM proteins (Munc18a, -b, and -c), each constitute a family of isoforms by which cognate partners form distinct SM/SNARE complexes that underlie the molecular basis of each exocytotic event in β-cells (1–3). Neuronal Munc18a/Syn-1A/SNAP25/VAMP2 complex mediating exocytosis of predocked insulin SGs (and predocked synaptic vesicles) (4,5) accounts for the first phase of the biphasic glucose-stimulated insulin secretion (GSIS). Newcomer insulin SGs are mobilized from the β-cell interior, taking minimal to no residence time at the plasma membrane (PM) before undergoing fusion (6,7). Newcomer SGs, accounting for almost all of second-phase GSIS and a major portion of first-phase GSIS, are mediated by another SM/SNARE complex, Munc18b/Syn-3/SNAP25/VAMP8 (8–10). The Munc18c/Syn-4 SM/SNARE complex exhibits redundant actions of mediating exocytosis of predocked and newcomer SGs (11).

This leaves Syn-2, which binds mainly Munc18b (also Munc18a but not Munc18c) (12), to be the only exocytotic syntaxin for which the role in exocytosis is yet to be elucidated. Peculiarly, Syn-2, also called epimorphin, was better studied for its morphogenic role influencing intestinal growth (13–15) and mammary carcinogenesis (16). Syn-2's role in exocytosis was reported in nonneuronal cells, including salivary (17) and pancreatic acini (18), sperm acrosome (19), lung alveoli (20), and platelets (21,22). An early report suggested that Syn-2 may not have a role in insulin secretion (23).

[1]Department of Medicine, University of Toronto, Toronto, Ontario, Canada
[2]Department of Medicine, Washington University School of Medicine in St. Louis, St. Louis, MO
[3]Department of Developmental Biology, Washington University School of Medicine in St. Louis, St. Louis, MO
[4]Department of Molecular Genetics, University of Toronto, Toronto, Ontario, Canada
Corresponding author: Herbert Y. Gaisano, herbert.gaisano@utoronto.ca.

Received 18 May 2016 and accepted 24 December 2016.

This article contains Supplementary Data online at http://diabetes.diabetesjournals.org/lookup/suppl/doi:10.2337/db16-0636/-/DC1.

D.Z., L.X., Y.K., and S.D. contributed equally to this study.

In this study, we determined Syn-2's role in insulin exocytosis using the Syn-2 knockout (Syn-2–KO) mouse (14,15). Paradoxically, Syn-2–KO mice exhibited improved glucose homeostasis from increased biphasic GSIS attributed to accelerated recruitment and fusion of newcomer SGs and, to a lesser extent, predocked SGs. Mechanistically, Syn-2 deletion resulted in increase in proexocytotic SM/SNARE complexes Syn-3/Munc18b/SNAP25/VAMP8 and Syn-1A/Munc18a/SNAP25/VAMP2. This suggests that Syn-2 likely acts as an inhibitory SNARE (24) in β-cells, which, when abrogated, relieves its competitive inhibition to enable formation of these profusion SNARE complexes to promote insulin secretion.

RESEARCH DESIGN AND METHODS

Mouse Genetics and Islet Isolation

Syn-2–KO (Epimorphin$^{-/-}$) mice were generated as described (14,15). All analyses in this paper on constitutive KO mice were performed with littermate control (wild-type [WT] mice). Animal procedures were performed in accordance with the University of Toronto Animal Care Committee's ethical guidelines. Islets were isolated by collagenase digestion and dispersed into single β-cells with Ca^{2+}/Mg^{2+}-free PBS containing 5 mmol/L EDTA and 0.25 mg/mL trypsin. Islets, β-cells, and INS-1 were cultured in supplemented RPMI 1640 (Gibco) medium.

Western Blot, Subcellular Fractionation, Immunoprecipitation, and In Vitro Binding Assays

Western blots of islet lysate samples were performed with the following antibodies: VAMP2 (1:2,000; Anson Lowe, Stanford University, Stanford, CA), VAMP8 (1:1,000; C.C. Wang and W.J. Hong, Institute of Molecular and Cell Biology, Singapore), Syn-1A (1:1,000; Sigma-Aldrich, St. Louis, MO), Syn-2 (1:1,200), Syn-3 (1:1,000), Syn-4 (1:1,200), and SNAP-23 (1:1,000) (Synaptic Systems, Goettingen, Germany); SNAP-25 (1:1,500; Sternberger Monoclonal, Covance, Princeton, NJ), Munc18a (1:1,000; BD Transduction Laboratories, San Jose, CA), Munc18b (1:1,000; V. Olkkonen, Minerva Foundation Institute, Finland), and Munc18c (1:800; D. Thurmond, City of Hope, Duarte, CA).

Subcellular fractionation was performed as previously reported (25) with slight modifications. Briefly, INS-1 cells at 70–80% confluence were washed and harvested into homogenization buffer containing protease inhibitors. Cells were disrupted and divided into two tubes of homogenates. The first tube was subjected to centrifugation at 900*g* (10 min) to remove the nuclei-enriched fraction; postnuclear supernatants were centrifuged at 5,500*g* (15 min), with subsequent supernatant centrifuged at 25,000*g* (20 min) to obtain the SG-enriched pellet; and the resulting supernatant was then centrifuged at 100,000*g* (1 h) to obtain the cytosolic fraction. From the second tube, PM fractions were obtained by centrifugation at 900*g*, the resulting supernatant then centrifuged at 100,000*g* (1 h) to obtain a pellet. The pellet was mixed with equal volumes of buffer A and buffer B, this mixture overlaid with buffer A, and centrifuged at 113,000*g* (1 h) to obtain an interface containing the PM fraction, which was collected and pelleted (3,000*g*, 10 min) to obtain the enriched PM fraction. All fractions were assayed for soluble protein content.

Immunoprecipitation (IP) assays using Syn-1A, -2, and -3 antibodies were conducted on adrenal glands (five to six glands per IP) from WT or Syn-2–KO mice or INS-1 cells transduced with Syn-2 small interfering RNA (siRNA) versus scramble control. Seventy-two–hour post-transduced cells were washed with PBS and incubated with Krebs-Ringer HEPES buffer (KRB; 30 min, 37°C) at 0.8 mmol/L glucose to obtain uniform basal condition and then further incubated with 10 nmol/L glucagon-like peptide 1 (GLP-1; 30 min) followed by stimulation with 16.7 mmol/L glucose (containing 10 nmol/L GLP-1) for 30 min. Treated cells were harvested and lysed by sonication in lysis buffer (25 mmol/L HEPES, 100 mmol/L KCl, 1.5% Triton X-100, and protease inhibitors). The detergent extract (650–800 μg protein) was precleared by incubation with 35 μL protein A agarose (50% slurry) for 1.5 h and then incubated with protein A agarose-crosslinked anti–Syn-1A, -2, or -3 Ab (2 μg) at 4°C for 1.5 h. Precipitated proteins were washed with IP buffer three times, separated on 12/15% SDS-PAGE, and identified with indicated antibodies.

In vitro binding assays were performed according to methods previously described (26). Briefly, glutathione *S*-transferase (GST) (as control), GST-VAMP2, or GST-VAMP8 (250 pmol protein) were bound to glutathione agarose beads and incubated with lysate extracts of transfected HEK293 cells (4°C, 2 h). Then the beads were washed three times with lysis buffer and samples separated on 13% SDS-PAGE. Proteins of interest were identified with specific antibodies.

Intraperitoneal Glucose Tolerance Test, Oral Glucose Tolerance Test, and Insulin Tolerance Test

Intraperitoneal glucose tolerance tests (IPGTT; 1 g glucose/kg body weight) were performed after 15- to 16-h fasting in 10- to 12-week-old male mice and weighed. Blood glucose was measured at indicated times and blood samples obtained at the same time point for insulin measurement. The plasma component of blood collected was assayed by insulin ELISA (Alpco Diagnostics, Salem, NH). Oral glucose tolerance test was performed as reported previously (10) (Supplementary Fig. 1*B*).

For insulin tolerance test, human biosynthetic insulin (Novo Nordisk, Toronto, Ontario, Canada) was injected intraperitoneally at a dose of 0.55 units/kg body weight into mice after a 5-h fasting period. Blood glucose was measured at indicated times following insulin administration.

Islet Perifusion and Static GSIS Assays

Batches of 50 mouse islets were stimulated with glucose in presence or absence of 10 nmol/L GLP-1 (7–36)-amide (Bachem, Torrance, CA) as indicated. This assay was performed as reported previously (10) with secreted insulin in perifusate fractions determined by radioimmunoassay

(kit from Linco Research, St. Charles, MO). Results are presented as insulin secreted normalized to total insulin content of the perifused islets collected at the end of each assay.

GSIS assays from INS-1 cells were performed as described previously (9). Insulin release and insulin content in INS-1 cell lysates were determined using a homogenous time-resolved fluorescence insulin assay (Cisbio), in accordance with the manufacturer's instructions, on a PHERAstar plate reader (BMG Labtech, Ortenberg, Germany). Insulin levels were normalized to total insulin content.

Confocal Immunofluorescence Microscopy

Pancreatic islet β-cells were treated as indicated, fixed, and then immunostained as described previously (10). Images were examined using a laser scanning confocal imaging system (LSM510; Carl Zeiss, Oberkochen, Germany). Measurement of mean fluorescence intensity was determined by NIS-Elements AR 3.0 (Nikon, Tokyo, Japan).

Electrophysiology

Cell membrane capacitance (Cm) was estimated by Lindau-Neher technique, implementing a "Sine-DC" feature of the lock-in module (40 mV peak-to-peak at 500-Hz frequency) in whole-cell configuration as previously described (11). Recordings were conducted using an EPC10 patch clamp amplifier equipped with Pulse and X-Chart software programs (HEKA Electronik, Lambrecht, Germany). Exocytotic events were elicited by a train of 10 500-ms depolarization pulses (1-Hz stimulation frequency) from −70 to 0 mV. All recordings were performed at 30°C. β-Cells were identified by their large size, measured electrophysiologically with an average Cm >6 pF as previously reported (27). Intracellular solution contained: 125 mmol cesium glutamate, 10 mmol CsCl, 10 mmol NaCl, 1 mmol $MgCl_2$, 5 mmol HEPES, 0.05 mmol EGTA, and 3 mmol MgATP (pH 7.2). The extracellular solution consisted of: 118 mmol NaCl, 5.6 mmol KCl, 1.2 mmol $MgCl_2$, 10 mmol $CaCl_2$, 20 mmol tetraethylammonium chloride, 5 mmol HEPES, and 5 mmol D-glucose (pH 7.4).

Total Internal Reflection Fluorescence Microscopy Imaging

Total internal reflection fluorescence microscopy (TIRFM) imaging was acquired by a TE2000U TIRF microscope (Nikon) at 5 Hz with a 100-ms exposure time as described previously (10,28). A monolayer of primary mouse β-cells was infected with adenovirus encoding neuropeptide Y (NPY)–EGFP and further cultured in 24-h before performing TIRFM. Before image acquisition, cells were preincubated for 30-min in basal 2.8 mmol/L glucose (in KRB) and then stimulated with 16.7 mmol/L glucose in presence or absence of 10 nmol/L GLP-1 as indicated at a flow rate of 1 mL/min or stimulated with 50 mmol/L KCl (pH 7.4, in KRB). Insulin granule mobilization and exocytosis were analyzed by MATLAB (Math Works, Natick, MA), ImageJ (National Institutes of Health), and Igor Pro (WaveMetrics, Lake Oswego, OR) software.

Fusion events indicated as flashes of fluorescence indicating NPY-EGFP cargo emptying were manually selected and assigned to one of three modes: predocked SGs that were visible before stimulation, no-dock newcomer SGs that fused without remaining at the PM for <200 ms (interval of one frame), and short-dock newcomer SGs that appeared during stimulation and stably remained for >200 ms before fusion occurs. An increase of EGFP fluorescence exceeding five times over the SD of the fluorescence fluctuation was considered as fusion events. Fluorescence of individual SGs was measured as mean brightness of the defined circle (1.335 μm in diameter). The number of predocked SGs was counted and averaged at the first 2 min prior to stimulation.

Islet Morphometry, Immunohistochemistry, and Immunofluorescence

Seven-micron–thick sections were obtained as we described previously (29) and then stained with insulin, glucagon (NovoCastra Laboratories; Leica Microsystems, Wetzlar, Germany), or Ki67 antibodies (Dako Diagnostics, Mississauga, Ontario, Canada). Total β-cell area, α-cell area, islet size, and islet number as well as total pancreatic area were determined on insulin-stained sections (10). Total β-cell area, α-cell area, and total islet number were calculated per total pancreatic area. Immunofluorescent-stained sections were visualized using an inverted fluorescence microscope (Carl Zeiss).

Statistical Analysis

All data are presented as mean ± SEM. Statistical significance was assessed by repeated-measures ANOVA or Student *t* test in SigmaStat (Systat Software, Inc). Significant difference is indicated by asterisks ($^*P < 0.05$, $^{**}P < 0.01$).

RESULTS

Syn-2 Deletion Increases Insulin Secretory Capacity and Improves Glucose Homeostasis but Has No Impact on β-Cell Mass

In pancreatic islets of WT mice (litter controls), Syn-2 colocalized mainly with β-cell insulin SGs (Fig. 1*A*), confirmed by subcellular fractionation (Fig. 1*B*), although small amounts of Syn-2 were in enriched PM fractions. In comparison, Syn-1A was most abundant in PM and Syn-3 in SGs. To begin to assess for a clinically relevant role of Syn-2 in insulin secretion, we examined for presence of Syn-2 in normal and type 2 diabetic (T2D) human islets (Fig. 1*C*). We confirmed that Syn-1A levels in T2D human islets were reduced (by 55%) (30). T2D islet Syn-3 levels were normal, but surprisingly, islet Syn-2 levels were also normal. We then studied the role of Syn-2 in insulin secretion, with the initial thinking that Syn-2 plays a profusion role in insulin SG exocytosis, perhaps redundant to Syn-1A and/or Syn-3.

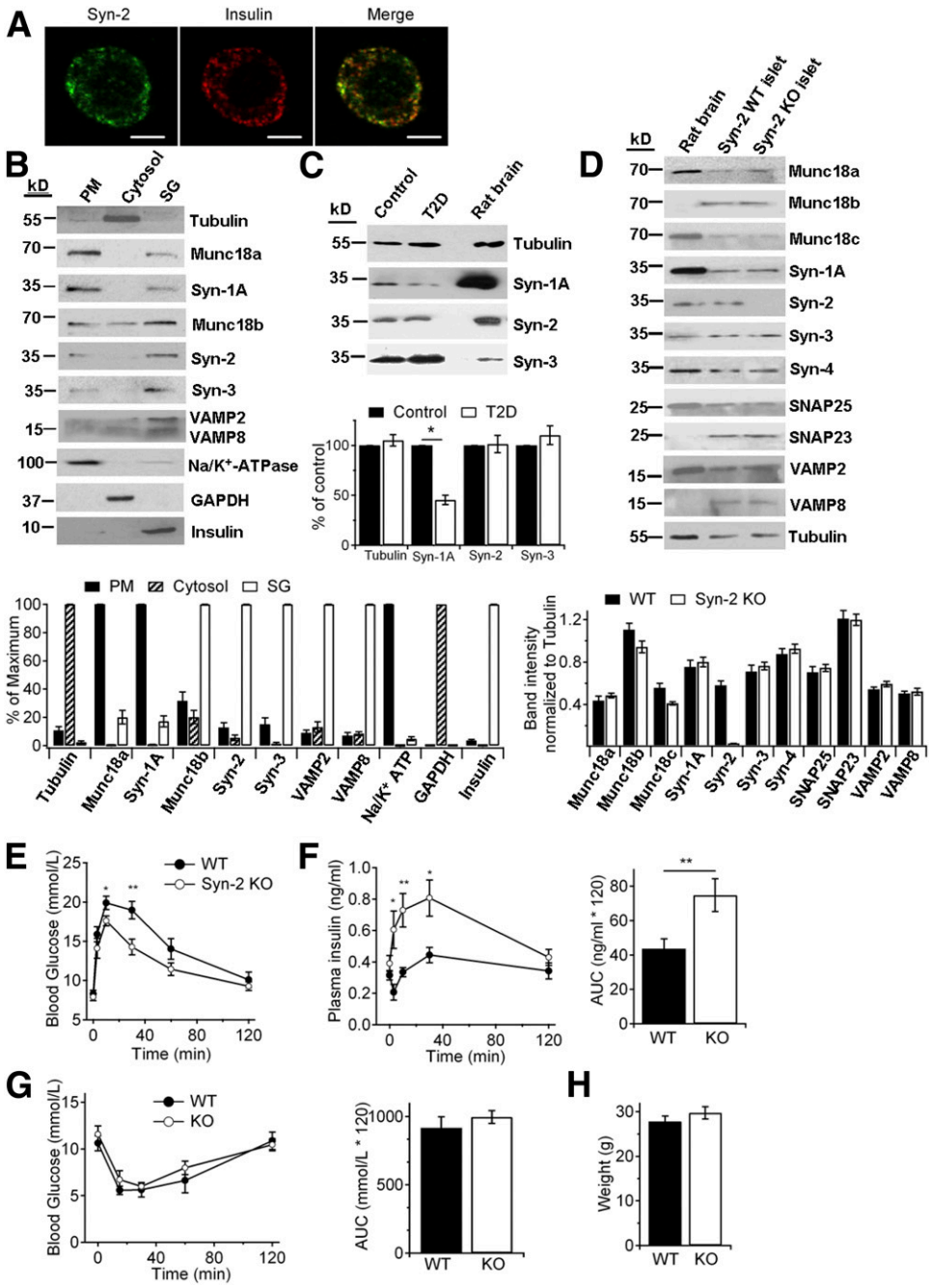

Figure 1—Syn-2 deletion improves GSIS and glucose homeostasis. *A:* Representative immunofluorescence images of Syn-2 (green) with insulin (red) in mouse pancreatic β-cells, with their colocalization shown in merge images (yellow). Shown are representative images of three independent experiments. Scale bars, 5 μm. *B:* Subcellular distribution (PM, 20 μg protein), cytosol (20 μg), and SG (20 μg) of Syn-1A, -2, -3, and their cognate SM proteins in INS-1 cells. Na^+/K^+-ATPase, GAPDH, and insulin were used as positive markers for PM, cytosol, and SG, respectively, to verify the purity of each fraction. For analysis ($N = 3$; bottom), the level in each fraction was expressed as a percentage of the signal of the strongest (maximum) band. *C:* Western blot (top) and analysis ($N = 3$; bottom) of syntaxin isoform levels in normal and T2D human pancreatic islets (25 μg protein). Rat brain (5 μg) was used as positive control. *D:* Western blot of SNARE and SNARE-associated protein levels in pancreatic islets of WT and Syn-2–KO mice (25 μg protein). Rat brain (5 μg) was used as positive and negative control. For analysis ($N = 3$; bottom), the level of each protein was normalized to the tubulin band. IPGTTs were performed with blood glucose levels in *E* and insulin secretion in *F* assessed during IPGTT. Insulin secretion is shown as AUC encompassing 120 min of IPGTT (*F*, right). $N = 19$/group. *G:* Blood glucose levels during IPGTT and corresponding AUC encompassing 120 min of IPGTT (right). $N = 8$/group. *H:* Weights of WT and Syn-2–KO mice used to perform IPGTT or insulin tolerance tests. Results are shown as mean ± SEM. $^*P < 0.05$; $^{**}P < 0.01$.

To assess for the endogenous role of Syn-2 in insulin secretion, we used a global Syn-2–KO mouse previously reported (14,15). Western blotting of islets from litter control WT and Syn-2–KO mice confirmed the absence of Syn-2, whereas levels of other exocytotic syntaxins, SNAP25, VAMPs, and SM proteins were not altered by Syn-2 deletion (Fig. 1*D*). Syn-2, which shares >60% homology to Syn-1A (31), was expected to reduce in vivo insulin secretory capacity when depleted, similar to Syn-1A deletion (5). Surprisingly, IPGTT showed that Syn-2–KO mice paradoxically exhibited better glucose tolerance (Fig. 1*E*), with corresponding higher plasma insulin levels (Fig. 1*F*). To negate a possible influence by insulin-sensitive tissues on glucose homeostasis, insulin tolerance tests exhibited comparable insulin sensitivity (Fig. 1*G*; area under the curve [AUC] in right panel); and weights of Syn-2–KO and WT mice used for in vivo studies were similar, suggesting no difference in food intake (Fig. 1*H*).

We explored for the reasons underlying how global Syn-2 deletion could explain the higher GSIS in vivo in the Syn-2–KO mice. Because Syn-2 affected morphogenesis of several tissues, a plausible explanation is that Syn-2 affected β-cell mass or islet architecture, which we reported for VAMP8 to which Syn-2 binds (10). Islets of 10-week-old Syn-2–KO and WT mice did not show any difference in β-cell area per pancreatic area, number, or size of islets, or Ki67-positive cells (Supplementary Fig. 1*A*). Islet architecture was not altered with α-cells remaining in the islet mantle and α-cell mass per pancreatic area unchanged (Supplementary Fig. 1*A*). These results exclude the possibility that Syn-2 depletion affects β-cell proliferation. A second explanation is that global Syn-2 deletion could affect intestinal release of incretin hormones GLP-1 and gastric inhibitory polypeptide (GIP) (32). In response to oral glucose tolerance test, fasting and peak plasma levels of total blood GLP-1 and GIP were not significantly different between WT and KO mice. In this study, we confirmed the better glucose tolerance and higher insulin levels in the Syn-2–KO mice (Supplementary Fig. 1*B*). A third reason is alteration in the release of glucagon from islet α-cells. However, instead of hyperglucagonemia, which would contribute to the observed hyperglycemia (33), we instead saw a mild reduction (only 17.5%) in fasting blood glucagon (Supplementary Fig. 1*C*). This is likely not attributed to a primary effect of Syn-2 deletion on α-cell glucagon secretion, but more likely because of the slightly higher (but insignificant) fasting glucose levels observed during the overnight fast (Fig. 1*F*).

Taken together, the improved glucose homeostasis in the global Syn-2–KO mice must be because of an increase in insulin release from each β-cell, leading us to the hypothesis that Syn-2 must be playing a negative regulatory role in insulin secretion. A corollary hypothesis that is of clinical relevance is that the normal levels of Syn-2 in T2D human islets might contribute to the reduced effectiveness of the already low islet levels of Syn-1A (30) on predocked SG fusion (5). Conversely, reducing islet Syn-2 levels could potentially relieve Syn-2 inhibition on insulin SG fusion, which could increase either Syn-1A actions on predocked SG fusion (5) or Syn-3 actions on newcomer SG fusion (9). These effects of β-cell Syn-2 depletion could potentially rescue the deficient biphasic GSIS in T2D human islets. We therefore focused the rest of our study to examine how Syn-2 depletion in β-cell could promote insulin SG exocytosis.

Syn-2 Deletion Enhanced Insulin Release by Increasing Priming and Mobilization of Insulin SG Pools

Physiologic biphasic GSIS was assessed by using islet perifusion assays in which Syn-2–KO islets compared with WT islets showed a 110% increase in first-phase (first 15 min) and 114% increase in second-phase (next 25 min) 16.7 mmol/L GSIS and an even greater increase of 272% in 10 nmol/L GLP-1 potentiation of 16.7 mmol/L GSIS (Fig. 2*A* and *B*). To confirm that this potentiated secretory response was attributed to Syn-2 depletion per se, we performed a rescue study in which Syn-2–KO islets were transduced with Ad-Syn-2–GFP (98% infection efficiency confirmed by GFP fluorescence) (Supplementary Fig. 2*A*), which reduced first-phase (by 48%) and second-phase GSIS (by 35%) (Fig. 2*B*) to comparable levels as WT mouse islets.

Exocytotic capacity of single β-cells was assessed by patch clamp Cm using serial depolarization (Fig. 2*C*), in which the first two pulses estimate the size of the readily releasable pool (RRP) that was previously purported to account for much of first-phase GSIS from whole islets and succeeding pulses (3rd–10th) measure RRP refilling purported to account for second-phase GSIS (34,35). Compared with WT β-cells, Cm increases in Syn-2–KO β-cells were increased at each depolarizing pulse (Fig. 2*D* and *E*), with the size of the RRP ($\Delta Cm_{1st-2nd}$ pulse) increased by 267% (23.5 ± 7.1 fF/pF; WT: 6.4 ± 1.5 fF/pF) and the rate of SG refilling ($\Delta Cm_{3rd-10th}$ pulse) increased by 172% (37.3 ± 10.1 fF/pF, WT: 13.6 ± 2.5 fF/pF). These results suggest that Syn-2 depletion increases depolarization-induced exocytosis by enhancing both priming and refilling of insulin SG pools.

Our previous work showed that Syn-1A and Syn-3 (36,37) directly bind and regulate calcium (Ca^{2+}) channels, which raised the possibility that Syn-2 effects on insulin secretion might in part be because of possible actions on Ca^{2+} channels or intracellular Ca^{2+} release. Glucose-evoked (16.7 mmol/L) (Supplementary Fig. 2*B*) and KCl (50 mmol/L) (Supplementary Fig. 2*C*) intracellular Ca^{2+} release was not different between Syn-2–KO or WT mouse β-cells. Furthermore, Syn-2 deletion in mouse β-cells did not affect voltage-gated Ca^{2+} currents (Supplementary Fig. 2*D*). These results taken together indicate that Syn-2 must be acting predominantly on the level of SG fusion.

Depletion of Syn-2 Recruits More Newcomer SGs to PM to Undergo Exocytosis and Promotes Fusion of Predocked SGs

Priming and refilling of SG pools have been attributed to sequential processes of docking of SGs onto PM, then

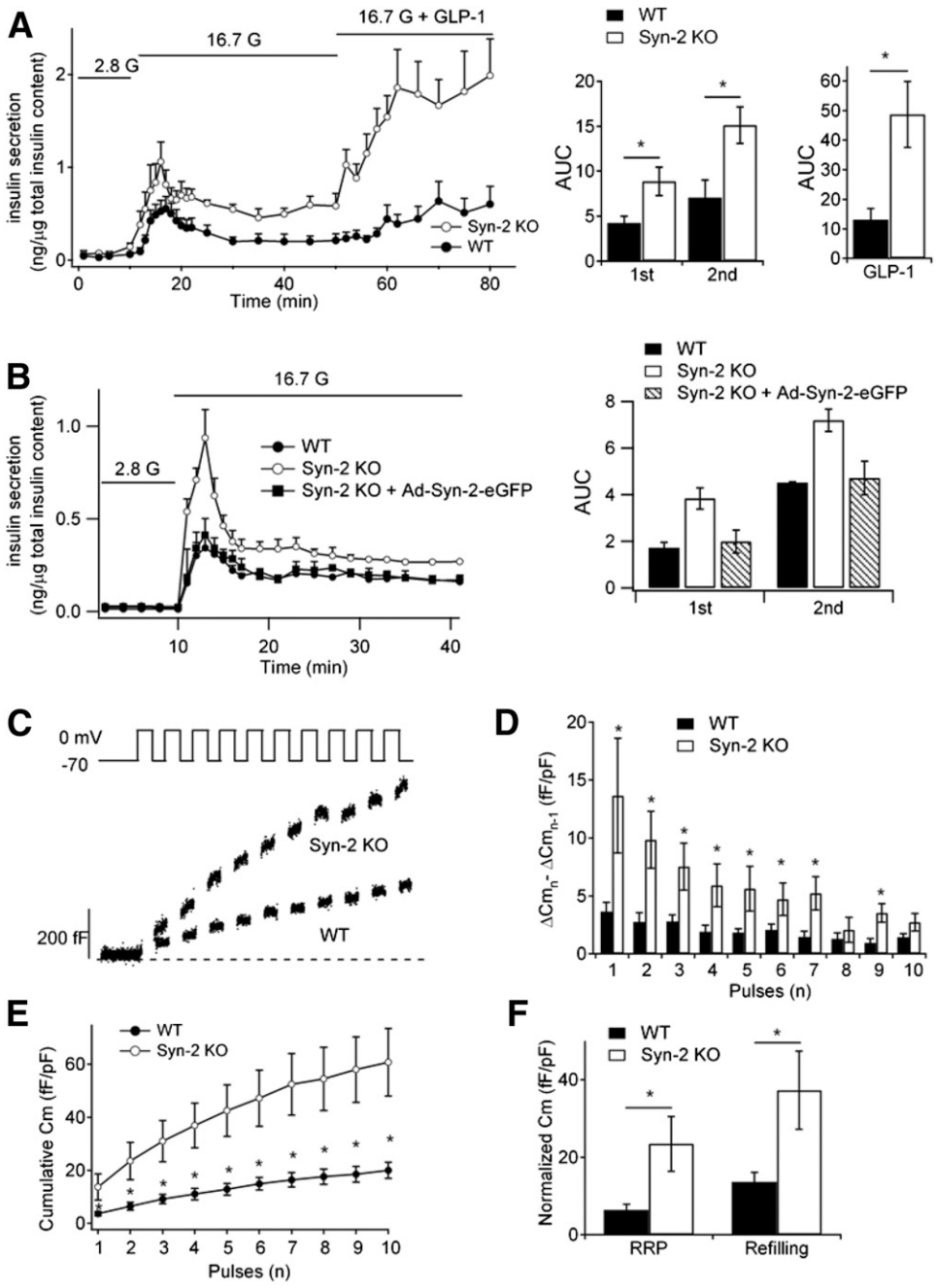

Figure 2—Syn-2 deletion increases biphasic insulin secretion. *A:* Islet perifusion assays in WT and Syn-2–KO mice pancreatic islets (left) and corresponding AUCs of insulin release (right) stimulated by 16.7 mmol/L glucose and then with application of GLP-1 (10 nmol/L). Data are from six independent experiments. *B:* Islet perifusion assays of Syn-2–KO mouse islets for which Syn-2 expression is restored by Ad-Syn-2–EGFP infection (Supplementary Fig. 2*A*); corresponding AUCs are shown on the right. *C:* Representative recordings of ΔCm during of a train of 500-ms depolarizations from −70 to 0 mV in WT and Syn-2–KO β-cells. Changes in cell Cm for each pulse in *D* and cumulative changes in Cm normalized to basal cell Cm (fF/pF) in *E* during a train of 10 500-ms depolarizations in WT (n = 20 cells) and Syn-2–KO (n = 18 cells) β-cells. *F:* Summary of Cm evoked by the first two pulses (pulses 1 and 2 represent the RRP) and the next eight pulses (pulses 3–10 represent SG mobilization). n = 18–20 cells. Summary graphs shown as mean ± SEM. *$P < 0.05$.

priming, in which predocked SGs sitting on PM for indefinite periods become ready for Ca^{2+}-triggered fusion. These processes revolve around assembly and disassembly of cognate SNARE and accessory proteins that bind Syn-1A (2). In fact, global deletion of Syn-1A reduced the number and fusion-competence of predocked insulin SGs (5). Now well described is the population of newcomer SGs that undergo little to no residence time at the PM before fusion, which accounts for a much larger portion of secretion in both first- and second-phase GSIS

(3,6,7,10). In fact, we had reported that newcomer SGs also contribute to the RRP as measured by patch clamp Cm (10). We used time-lapse TIRFM to track exocytosis dynamics of insulin SGs tagged by adenovirus transduction of NPY-EGFP. At the unstimulated (2.8 mmol/L glucose) state (Fig. 3*A*), punctate fluorescence indicating docked SGs was not different between WT (10.4 ± 1.34/100 μm^2) and KO β-cells (11.7 ± 0.70/100 μm^2). When stimulated with 16.7 mmol/L glucose plus 10 nmol/L GLP-1, assessment of cumulative fusion events over time (Fig. 3*B*) showed much more fusion events during the 20-min acquisition in Syn-2–KO β-cells.

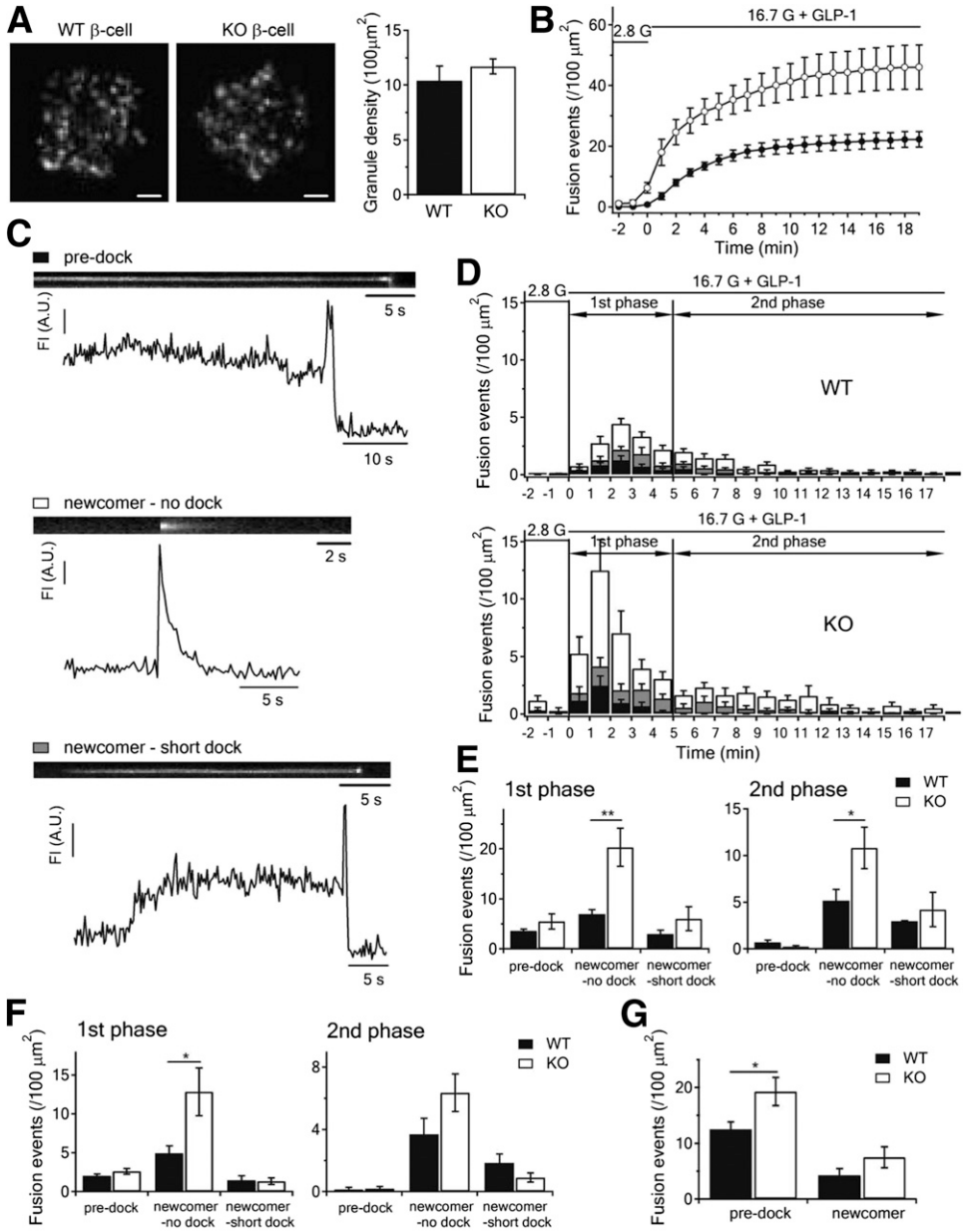

Figure 3—Syn-2 deletion increases newcomer SG exocytosis during biphasic GSIS. *A:* TIRFM images of docked insulin SGs in WT or Syn-2–KO β-cells (left). Scale bars, 2 μm. Averaged SG densities before stimulation (right). *B:* Cumulative insulin SG fusion events per cell per 100 μm^2 stimulated as indicated. *C:* Kymographs and corresponding fluorescence intensity (FI) curves showing three modes of insulin SG fusion events: predock (black bar), newcomer-no dock (white bar), and newcomer short-dock (gray bar). *D:* Histogram of fusion events in first (first 5 min after 16.7 mmol/L glucose plus 10 nmol/L GLP-1 stimulation) and second phases (5–18 min) in WT versus KO β-cells. Data obtained from four independent experiments (three to five cells from each experiment). Summary of the three modes of fusion events in first (left) and second phases (right) stimulated by 16.7 mmol/L glucose plus 10 nmol/L GLP-1 in *E* or by 16.7 mmol/L glucose in *F*. For corresponding histogram of fusion events for *F*, see Supplementary Fig. 3*A*. *G:* Summary of predocked and newcomer fusion events stimulated by 50 mmol/L KCl. For corresponding histogram of fusion events, see in Supplementary Fig. 3*B*. Summary graphs shown as mean ± SEM. **P* < 0.05; ***P* < 0.01. A.U., arbitrary units.

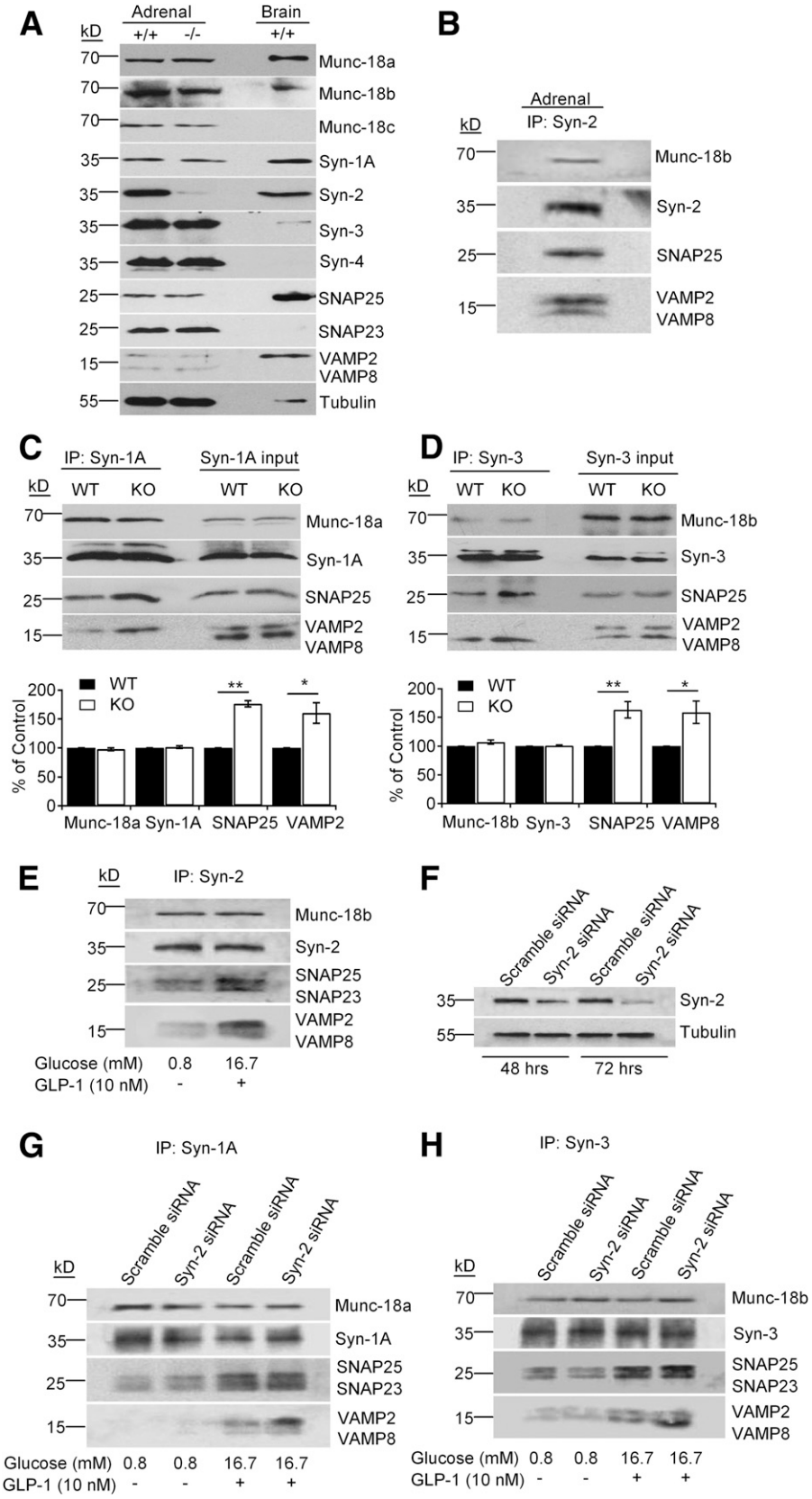

Figure 4— Syn-2 deletion enables formation of more profusion SM/SNARE complexes. *A:* SM/SNARE protein profile of adrenal glands from WT and Syn-2–KO mice. *B:* Syn-2 co-IP of cognate SM/SNARE proteins in WT adrenal gland lysates. Representative of two experiments. Co-IP of Syn-1A in *C* or Syn-3 in *D* pulled down SM/trans-SNARE complexes from WT versus Syn-2–KO mice adrenal glands. Representative of three independent experiments with samples performed in duplicate; respective densitometry analyses shown in bottom panels. Values from WT adrenals were used as control (100%); all other values were normalized to control. *E:* Syn-2 co-IP of cognate

We dissected the single SG fusion dynamics. At 2.8 mmol/L glucose, we seldom found spontaneous fusion events. When 16.7 mmol/L glucose was added after preincubation with 10 nmol/L GLP-1 to potentiate insulin exocytosis, SG fusion events were observed as flashes of fluorescence that rapidly dissipate in a cloudlike diffusion pattern. These exocytotic events were not uniform and could be categorized into three distinct modes (Fig. 3*C*) (10). Even in first-phase GSIS, newcomer SGs already accounted for >70% of exocytotic events in WT β-cells (Fig. 3*D*, top panel), which corresponded to the diverging cumulative increase in exocytosis in WT compared with Syn-2–KO β-cells (Fig. 3*B*). Enhancement of exocytosis in both phases of GSIS evoked by 16.7 mmol/L glucose plus GLP-1 was accounted for entirely from potentiation in recruitment and fusion of no-dock newcomer SGs (WT: 6.96 ± 0.87 vs. KO: 20.30 ± 4.8/100 μm^2 in first-phase; WT: 5.16 ± 1.20 vs. KO: 10.80 ± 2.61/100 μm^2 in second-phase) (Fig. 3*E*), as fusion of predock SGs were similar between WT and KO β-cells. There was no change in short-dock newcomer SGs. For a more critical assessment, we assessed exocytosis evoked by 16.7 mmol/L glucose only or by 50 mmol/L K^+ stimulation, which the latter causes fusions of predocked SGs predominantly. Glucose-only stimulation caused similar trends as we saw with GLP-1–potentiated GSIS with a predominant increase in fusion of no-dock newcomer SGs (Fig. 3*F* and Supplementary Fig. 3*A*). However, KCl stimulation showed a dramatic preferential enhancement of predocked SG fusion in Syn-2–KO β-cells (WT: 12.5 ± 1.36 vs. KO: 19.3 ± 2.52/100 μm^2) (Fig. 3*G* and Supplementary Fig. 3*B*), consistent with the larger depolarization-evoked RRP (predominantly predocked SG) exocytosis in the Cm study (Fig. 2*C*–*F*). These results indicate that Syn-2 may be acting as a clamp that blocks recruitment and exocytosis of no-dock newcomer and predocked SGs (to lesser extent), which, when relieved by Syn-2 depletion, then allows both no-dock newcomer and predocked SGs to proceed to fusion. These results are reminiscent of Syn-3 (9) and VAMP8 (10) overexpression which promoted recruitment and exocytosis of no-dock newcomer SGs, suggesting that Syn-2 might act as negative regulator (i.e., inhibitory SNARE) against Syn-3/VAMP8 and Syn-1A/VAMP2 profusion complexes.

Absence of Syn-2 Enables Formation of More Profusion SNARE Complexes

Syn-1A forms a complex primarily with VAMP2, with the complete SM/SNARE complex including Munc18a and SNAP25, to mediate exocytosis of predocked SG (2). In contrast, the putative SM/SNARE complex that mediates newcomer SGs is formed by Munc18b (8), Syn-3 (9), VAMP8 (10), and SNAP25. Peculiarly, in those studies, we also noted the formation of Syn-2 complexes with Munc18b and SNAP25, binding both VAMP2 and VAMP8. This led us to postulate that Syn-2's inhibitory role in exocytosis might be as a negative regulator that binds the two VAMPs in competition with their respective profusion Syn-1A (5) and Syn-3 (9). Because pancreatic islets provide insufficient protein required for co-IP assays, we used two surrogates: endocrine adrenal glands of the same animals experimented above, which have a very similar profile of exocytotic proteins as pancreatic islets (Fig. 4*A*), and Syn-2 siRNA-treated insulinoma INS-1 cells. In WT mice, Syn-2 antibody co-IP Munc18b, SNAP25, and SNAP23 and both VAMP2 and VAMP8 from adrenal gland lysates (Fig. 4*B*) were used. Although there was no change in adrenal gland protein levels of Syn-1A and Syn-3 SNARE/SM complexes, co-IP with Syn-1A and Syn-3 antibodies coprecipitated more of their respective SM/SNARE complexes from Syn-2–KO mice than WT mice adrenal glands (Fig. 4*C* and *D*). Specifically, Syn-2 deletion enabled Syn-1A to pull down more SNAP25 (76% increase) and VAMP2 (61% increase) (Fig. 4*C*); Syn-3 similarly pulled down more SNAP25 (63% increase) and VAMP8 (59% increase) (Fig. 4*D*).

INS-1, a β-cell surrogate we have used for such studies, upon stimulation with 16.7 mmol/L glucose plus 10 nmol/L GLP-1, activated formation of SM/SNARE complexes, by which at basal state (0.8 mmol/L glucose), SM proteins bind syntaxins in closed conformation that has reduced capacity to form SNARE complexes. We confirmed that Syn-2 antibody co-IP the same proteins from stimulated INS-1 (8,10), including VAMP2 and VAMP8 (Fig. 4*E* and Supplementary Fig. 4*D*). We then depleted Syn-2 in INS-1 cells with siRNA by 72.2% at 48 h and 83.8% at 72 h (Fig. 4*F* and Supplementary Fig. 4*B*) to assess whether this affects profusion Syn-1A and Syn-3 SNARE complexes. We confirmed their effects on insulin secretion, which showed enhanced GSIS (16.7 mmol/L glucose) in absence (by 51%) or presence of 10 nmol/L GLP-1 (by 54%) (Supplementary Fig. 4*A* and *C*). At basal state, Syn-1A and Syn-3 in both Syn-2 siRNA- and scramble siRNA-treated INS-1 cells bind similar amounts of cognate Munc18a and Munc18b, respectively, and similarly small amounts of SNAP25 (and SNAP23), but very little VAMPs were co-IP (Fig. 4*G* and *H*). On stimulation, Syn-1A (Fig. 4*G* and Supplementary Fig. 4*E*) and Syn-3

SNARE/SM proteins in control INS-1 cells, treated as indicated; analysis in Supplementary Fig. 4*D*. *F:* Syn-2 siRNA knockdown in INS-1 cells compared with scrambled siRNA. Representative of three experiments; analysis in Supplementary Fig. 4*A* and *B* (protein levels) and Supplementary Fig. 4*C* (insulin secretion). *G* and *H:* Co-IP of Syn-1A in *G* or Syn-3 in *H* pulled down cognate SNARE/SM proteins in Syn-2 siRNA versus control scrambled nonsense siRNA-transduced INS-1 cells, treated as indicated. Representative of three independent experiments with samples performed in duplicate; analysis in Supplementary Fig. 4*E* and *F*. $^*P < 0.05$; $^{**}P < 0.01$.

(Fig. 4*H* and Supplementary Fig. 4*F*) bind similarly more SNAP25 and SNAP23. However, from Syn-2–depleted cells, Syn-1A pulled down more VAMP2 (by 93.4%), and Syn-3 pulled down more VAMP8 (by 81.7%) than scrambled siRNA-treated cells.

These adrenal gland (Fig. 4*A–D*) and INS-1 results (Fig. 4*E–H*) were very comparable, which, taken together, indicate that endogenous Syn-2 reduces the capacity of Syn-1A and Syn-3 to form profusion SM/SNARE complexes with VAMP2 and VAMP8, respectively, thus acting as an inhibitory SNARE (24) that blocks exocytosis mediated by these SM/SNARE complexes. To assess this more critically on whether Syn-2 competes against Syn-1A and Syn-3 for binding to v-SNAREs, Syn-2 was coexpressed with Syn-1A or Syn-3 in HEK cells and subjected to pull down with GST-VAMP2 or GST-VAMP8 (Fig. 5). Syn-2 potently reduced Syn-3 binding to cognate VAMP8 by 67.4%, providing the mechanism by which Syn-2 deletion in β-cells promoted newcomer SG fusion (Fig. 3) by increasing Syn-3 SM/SNARE complex formation (Fig. 4). Syn-2 also inhibited Syn-1A binding to cognate VAMP2 but more moderately by 35.2% (Fig. 5), suggesting that Syn-2 depletion could (albeit perhaps less effectively) promote fusion of predocked SGs. Thus, therapeutically inducing Syn-2 depletion in T2D β-cells would greatly potentiate newcomer SG fusion in both first- and second-phase GSIS since islet Syn-3 levels remained normal (Fig. 1*C*); and perhaps also enable the reduced levels of Syn-1A (Fig. 1*C*) to more effectively promote and at least partially restore predocked SG fusion in first-phase GSIS. Interestingly, Syn-2 also reduced Syn-3 promiscuous binding to VAMP2 by 55.9% and Syn-1A promiscuous binding to VAMP8 by 43.5%.

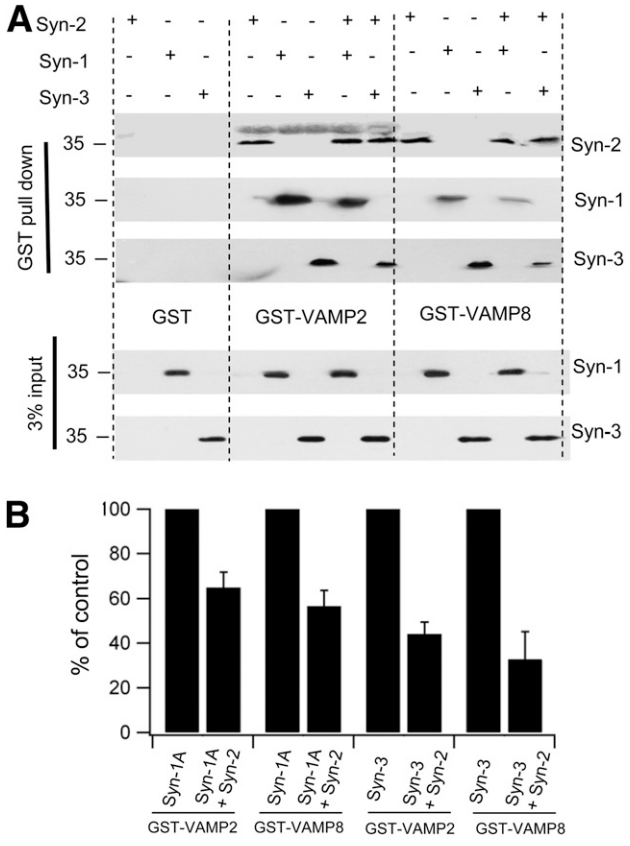

Figure 5—Syn-2 blocks Syn-3 and Syn-1A binding to VAMP8 and VAMP2. *A*: HEK cells were transfected with Syn-1A, Syn-2, or Syn-3 alone or Syn-2 cotransfected with Syn-1A or Syn-3. At 48 h after transfection, cells were collected, and GST (as negative control), GST-VAMP2, or GST-VAMP8 was used to pull down Syn-1A, Syn-2, and Syn-3 from the cell lysate extracts. Shown is a representative of three separate experiments, by which the percentage recovery of total protein for Syn-1A alone is 3.02 ± 0.56% and Syn-3 alone is 2.88 ± 1.01%. *B*: Analysis of the three experiments. For direct comparison of the three experiments, the results were normalized to the percentage of Syn-A or Syn-3 use alone (control) performed in each experiment.

DISCUSSION

Inhibitory SNAREs, demonstrated by in vitro lipid fusion assays to form nonfusogenic complexes, were postulated to provide a countercurrent fusion pattern within Golgi stacks (24) and subsequently shown in bacteria to block the fusion of infectious phagosomes with endocytic compartments containing degradative enzymes (38). We demonstrated in this study this concept of inhibitory SNAREs to be applicable to mammalian cells in modulating insulin exocytosis that profoundly influences whole-animal glucose homeostasis. This apparent deliberate mechanism to reduce efficiency of exocytosis adds to the plasticity of some secretory cells in which a slower secretory process (than neurons) of hormone release is required to respond to nutrient absorption. Along this thinking, it is possible that Syn-2 might not be a pure inhibitory SNARE per se but rather an inefficient fusion protein that serves the extremely slow exocytosis in some nonneuronal cells such as pancreatic acinar cells (18) to enable metered release of digestive enzymes over several hours required to complete food digestion after a meal. Syn-2's role as a pro- or inhibitory SNARE may thus be cell context specific; and in islet β-cells, Syn-2 might be a decelerator target membrane SNARE that brakes the efficient fusogenic Syn-1A and Syn-3. A release of the Syn-2 "brake" in secretory-deficient T2D β-cells exhibiting reduced levels of profusion SNARE proteins (1,3,30) could be a therapeutic strategy to improve GSIS in diabetes.

Syn-2 depletion seems to have strong effects on increasing newcomer SG fusion mediated by Syn-3 (9) after glucose (and GLP-1–potentiated) stimulation, which is explained at least in part by the stronger affinity of Syn-2 than Syn-3 for newcomer SG v-SNARE VAMP8 (10). Syn-2 depletion resulted in lesser increase in fusion of predocked SGs mediated by Syn-1A, unless selectively evoked by high KCl concentration. The latter may be because the pool of primed predocked SGs is limited in normal β-cells (even less in diabetic β-cells), which may already be saturated with preassembled Syn-1A SM/SNARE complexes, with Syn-1A having a higher affinity

for predocked SG v-SNARE VAMP2 than Syn-2. KCl stimulation, more likely to recruit additional Syn-1A SM/SNARE complexes than glucose stimulation, may explain its receptiveness to Syn-2 depletion. The much bigger pool of newcomer SGs requires continuous new assembly of Syn-3 SM/SNARE complexes to sustain second-phase GSIS (and GLP-1 potentiation), which is more receptive to Syn-2 depletion. β-Cell Syn-2 depletion thus presents a favorable target for therapeutic intervention in combination with incretin or sulfonylurea treatments, particularly in the background of reduced SNARE protein levels in diabetic β-cells (30).

More work will be needed to elucidate the putative domains within Syn-2 that confer its feature of slower fusion or fusion block compared with Syn-1A and Syn-3, which share >60% amino acid identity with Syn-2 (31). Such comparative structural-function insights between these syntaxins could reveal the distinct features of Syn-1A mediating the prerequisite SG docking, which Syn-3 seems to circumvent in mediating fusion of newcomer SGs with minimal residence time at the PM. Perhaps the SNARE complexes formed by the three syntaxins zipper up very differently when mediating membrane fusion (39,40), and maybe with Syn-2, the zipper somehow gets "stuck."

Acknowledgments. The authors thank E. Kwan and X. Lin (Department of Medicine, University of Toronto, Toronto, Canada) for technical assistance.

Funding. This work was supported by the Canadian Institutes of Health Research (MOP-89889 and MOP-86544), and postdoctoral fellowship support was provided by the Banting & Best Diabetes Centre, University of Toronto (to D.Z.), the Canadian Association of Gastroenterology and Canadian Institutes of Health Research (to S.D.), and the Canadian Diabetes Association (to L.X.).

Duality of Interest. No potential conflicts of interest relevant to this article were reported.

Author Contributions. D.Z. and H.Y.G. formulated the original hypothesis and worked on the manuscript revision. D.Z. performed TIRFM imaging. D.Z. and J.B.H. performed the animal experiments. D.Z. and T.Q. performed islet perifusion assays. D.Z. and T.L. performed confocal imaging. L.X. helped in drafting the manuscript and conducted electrophysiology studies. Y.K., S.D., and H.X. were responsible for protein-binding and Western blot studies. D.C.R. made the Syn-2–KO mouse. D.C.R., L.O., and H.Y.G. contributed to the DISCUSSION. All authors discussed the results. H.Y.G. is the guarantor of this work and, as such, had full access to all the data in the study and takes responsibility for the integrity of the data and the accuracy of the data analysis.

References

1. Kwan EP, Gaisano HY. Rescuing the subprime meltdown in insulin exocytosis in diabetes. Ann N Y Acad Sci 2009;1152:154–164

2. Südhof TC, Rothman JE. Membrane fusion: grappling with SNARE and SM proteins. Science 2009;323:474–477

3. Gaisano HY. Deploying insulin granule-granule fusion to rescue deficient insulin secretion in diabetes. Diabetologia 2012;55:877–880

4. Oh E, Kalwat MA, Kim MJ, Verhage M, Thurmond DC. Munc18-1 regulates first-phase insulin release by promoting granule docking to multiple syntaxin isoforms. J Biol Chem 2012;287:25821–25833

5. Ohara-Imaizumi M, Fujiwara T, Nakamichi Y, et al. Imaging analysis reveals mechanistic differences between first- and second-phase insulin exocytosis. J Cell Biol 2007;177:695–705

6. Kasai K, Fujita T, Gomi H, Izumi T. Docking is not a prerequisite but a temporal constraint for fusion of secretory granules. Traffic 2008;9:1191–1203

7. Shibasaki T, Takahashi H, Miki T, et al. Essential role of Epac2/Rap1 signaling in regulation of insulin granule dynamics by cAMP. Proc Natl Acad Sci U S A 2007;104:19333–19338

8. Lam PP, Ohno M, Dolai S, et al. Munc18b is a major mediator of insulin exocytosis in rat pancreatic β-cells. Diabetes 2013;62:2416–2428

9. Zhu D, Koo E, Kwan E, et al. Syntaxin-3 regulates newcomer insulin granule exocytosis and compound fusion in pancreatic beta cells. Diabetologia 2013;56:359–369

10. Zhu D, Zhang Y, Lam PP, et al. Dual role of VAMP8 in regulating insulin exocytosis and islet β cell growth. Cell Metab 2012;16:238–249

11. Xie L, Zhu D, Dolai S, et al. Syntaxin-4 mediates exocytosis of pre-docked and newcomer insulin granules underlying biphasic glucose-stimulated insulin secretion in human pancreatic beta cells. Diabetologia 2015;58:1250–1259

12. Tellam JT, McIntosh S, James DE. Molecular identification of two novel Munc-18 isoforms expressed in non-neuronal tissues. J Biol Chem 1995;270:5857–5863

13. Fritsch C, Swietlicki EA, Lefebvre O, et al. Epimorphin expression in intestinal myofibroblasts induces epithelial morphogenesis. J Clin Invest 2002;110:1629–1641

14. Shaker A, Swietlicki EA, Wang L, et al. Epimorphin deletion protects mice from inflammation-induced colon carcinogenesis and alters stem cell niche myofibroblast secretion. J Clin Invest 2010;120:2081–2093

15. Wang Y, Wang L, Iordanov H, et al. Epimorphin(-/-) mice have increased intestinal growth, decreased susceptibility to dextran sodium sulfate colitis, and impaired spermatogenesis. J Clin Invest 2006;116:1535–1546

16. Bascom JL, Fata JE, Hirai Y, Sternlicht MD, Bissell MJ. Epimorphin overexpression in the mouse mammary gland promotes alveolar hyperplasia and mammary adenocarcinoma. Cancer Res 2005;65:8617–8621

17. Fukuda M, Imai A, Nashida T, Shimomura H. Slp4-a/granuphilin-a interacts with syntaxin-2/3 in a Munc18-2-dependent manner. J Biol Chem 2005;280:39175–39184

18. Pickett JA, Thorn P, Edwardson JM. The plasma membrane Q-SNARE syntaxin 2 enters the zymogen granule membrane during exocytosis in the pancreatic acinar cell. J Biol Chem 2005;280:1506–1511

19. Hutt DM, Baltz JM, Ngsee JK. Synaptotagmin VI and VIII and syntaxin 2 are essential for the mouse sperm acrosome reaction. J Biol Chem 2005;280:20197–20203

20. Abonyo BO, Gou D, Wang P, Narasaraju T, Wang Z, Liu L. Syntaxin 2 and SNAP-23 are required for regulated surfactant secretion. Biochemistry 2004;43:3499–3506

21. Chen D, Lemons PP, Schraw T, Whiteheart SW. Molecular mechanisms of platelet exocytosis: role of SNAP-23 and syntaxin 2 and 4 in lysosome release. Blood 2000;96:1782–1788

22. Lemons PP, Chen D, Whiteheart SW. Molecular mechanisms of platelet exocytosis: requirements for alpha-granule release. Biochem Biophys Res Commun 2000;267:875–880

23. Nagamatsu S, Sawa H, Nakamichi Y, Kondo Y, Matsushima S, Watanabe T. Non-functional role of syntaxin 2 in insulin exocytosis by pancreatic beta cells. Cell Biochem Funct 1997;15:237–242

24. Varlamov O, Volchuk A, Rahimian V, et al. i-SNAREs: inhibitory SNAREs that fine-tune the specificity of membrane fusion. J Cell Biol 2004;164:79–88

25. Nevins AK, Thurmond DC. A direct interaction between Cdc42 and vesicle-associated membrane protein 2 regulates SNARE-dependent insulin exocytosis. J Biol Chem 2005;280:1944–1952

26. Kang Y, Leung YM, Manning-Fox JE, et al. Syntaxin-1A inhibits cardiac KATP channels by its actions on nucleotide binding folds 1 and 2 of sulfonylurea receptor 2A. J Biol Chem 2004;279:47125–47131

27. Göpel S, Kanno T, Barg S, Galvanovskis J, Rorsman P. Voltage-gated and resting membrane currents recorded from B-cells in intact mouse pancreatic islets. J Physiol 1999;521:717–728

28. Xie L, Zhu D, Gaisano HY. Role of mammalian homologue of Caenorhabditis elegans unc-13-1 (Munc13-1) in the recruitment of newcomer insulin granules in

both first and second phases of glucose-stimulated insulin secretion in mouse islets. Diabetologia 2012;55:2693–2702
29. Choi D, Schroer SA, Lu SY, et al. Erythropoietin protects against diabetes through direct effects on pancreatic beta cells. J Exp Med 2010;207:2831–2842
30. Ostenson CG, Gaisano H, Sheu L, Tibell A, Bartfai T. Impaired gene and protein expression of exocytotic soluble N-ethylmaleimide attachment protein receptor complex proteins in pancreatic islets of type 2 diabetic patients. Diabetes 2006;55:435–440
31. Bennett MK, García-Arrarás JE, Elferink LA, et al. The syntaxin family of vesicular transport receptors. Cell 1993;74:863–873
32. Lovshin JA, Drucker DJ. Incretin-based therapies for type 2 diabetes mellitus. Nat Rev Endocrinol 2009;5:262–269
33. Gaisano HY, Macdonald PE, Vranic M. Glucagon secretion and signaling in the development of diabetes. Front Physiol 2012;3:349
34. Rorsman P, Renström E. Insulin granule dynamics in pancreatic beta cells. Diabetologia 2003;46:1029–1045
35. Kwan EP, Xie L, Sheu L, Ohtsuka T, Gaisano HY. Interaction between Munc13-1 and RIM is critical for glucagon-like peptide-1 mediated rescue of exocytotic defects in Munc13-1 deficient pancreatic beta-cells. Diabetes 2007; 56:2579–2588
36. Xie L, Dolai S, Kang Y, et al. Syntaxin-3 binds and modulates both R- and L-type calcium channels in insulin-secreting INS-1 832/13 cells. PLoS One 2016; 11:e0147862
37. Kang Y, Huang X, Pasyk EA, et al. Syntaxin-3 and syntaxin-1A inhibit L-type calcium channel activity, insulin biosynthesis and exocytosis in beta-cell lines. Diabetologia 2002;45:231–241
38. Paumet F, Wesolowski J, Garcia-Diaz A, et al. Intracellular bacteria encode inhibitory SNARE-like proteins. PLoS One 2009;4:e7375
39. Gao Y, Zorman S, Gundersen G, et al. Single reconstituted neuronal SNARE complexes zipper in three distinct stages. Science 2012;337:1340–1343
40. Shi L, Shen QT, Kiel A, et al. SNARE proteins: one to fuse and three to keep the nascent fusion pore open. Science 2012;335:1355–1359